Dalton Transactions

Accepted Manuscript

ROYAL SOCIETY OF CHEMISTRY

www.rsc.org/dalton

Influence of para substituents in controlling photophysical behavior and different non-covalent weak interactions in zinc complexes of a phenol based "End-off" compartmental ligand†

Prateeti Chakraborty, [a] Jaydeep Adhikary, [a] Sugata Samanta, [b] Ishani Majumder, [a] Chiara Massera, [c] Daniel Escudero, *[, d] Sanjib Ghosh,*[, b] Antonio Bauza, [e] Antonio Frontera*[,e]and Debasis Das*[,a]

[a]Department of Chemistry, University of Calcutta, 92 A. P. C. Road, Kolkata-700 009, India, E-mail: dasdebasis2001@yahoo.com

[b]Department of Chemistry, Presidency University, Kolkata-700073, India, E-mail: pchemsg@gmail.com

[c] Dipartimento di Chimica, University of Parma, Viale delle Scienze 17/A, 43124 Parma, Italy

[d] Chimie Et Interdisciplinarité, Synthèse, Analyse, Modélisation (CEISAM), UMR CNRS no. 6320, BP 92208, Université de Nantes, 2, Rue de la Houssinière, 44322 Nantes, Cedex 3, France. E-mail: daniel.escudero@univ-nantes.fr

[e] Departament de Química, Universitat de les Illes Balears, Crta. de Valldemossa km 7.5, 07122 Palma (Baleares), Spain, E-mail: toni.frontera@uib.es

† Electronic supplementary information (ESI) available. See DOI: XX

Three dinuclear zinc(II) complexes with "end-off" compartmental ligands, namely 2,6-bis(*N*-ethylmorpholine-iminomethyl)-4-R-phenol (R=-CH_3, Cl, ^{t}Bu) have been synthesized with the aim of exploring the role of the para substituent present in ligand backbone in controlling the structural diversity, photophysical property and different weak interactions of the complexes. All the three species, with general formula {2[$Zn_2L(CH_3COO)_2$][$Zn(NCS)_4$]}, show the complex anion $Zn(NCS)_4^{2-}$ as common structural feature decisive for crystallization. Amusingly, all of them possess several non-covalent weak interactions where the nature of the "R" group plays an essential role as exposed by DFT study. Besides exhibiting fluorescence behavior the complexes also show para substitution controlled phosphorescence both at room and low temperature. Anisotropy studies suggest the existence of complex **2** and **3** as dimers in solution. The origins of the unusual room temperature phosphorescence and

fluorescence behavior of the complexes have been rationalized in the light of theoretical calculations.

Introduction

Zinc which was regarded as a boring [1] and featureless element has become of focal interest to the coordination chemists in recent years mainly for its amazing bio-compatibility.[2-8] Although zinc is the second most abundant trace element next to iron in bio-system and ubiquitous in nature, it has only recently attracted the attention of chemists with the advancement of emission spectroscopy.[9] Actually, zinc is silent towards all common spectroscopic techniques, and that may be one of the main reasons for late development of zinc biochemistry and consequently zinc coordination chemistry. However, zinc has the ability to greatly enhance photo-luminescence efficiency of organic luminescent ligands, efficiency that can be controlled tuning the steric and/or electronic properties of the ligand.[10-14] In this respect, Schiff bases are among the most fascinating ligands for the coordination chemists because of their straightforward synthesis and easy tuning of steric and electronic properties depending on one's desire and requirements.[15-19] Interestingly, photoluminescence studies of Zn-Schiff-base system (Zn-SB) are not so well-explored as it is with other ligand systems. Moreover, in many of the cases the origin of the observed photoluminescence properties is not thoroughly authenticated which demands in depth theoretical calculations. Presently, phenol based "end-off" compartmental ligands are considered attractive and versatile Schiff bases for several reasons. A few interesting reports can be found in the literature, where "end-off" compartmental ligands have been used as sensor for Zn ions, exploiting the enhanced fluorescence efficiency after complexation.[20-22] However, detailed studies of the role of substituent present on the periphery of ligand back bone in influencing the fluorescence property of zinc complexes, both from an experimental and theoretical point of view are scanty. We have therefore carried out this work with the aim to investigate the role of para substituents (R) of phenol based "end-off" compartmental ligands on structural and photoluminescence properties of zinc complexes. We report the syntheses of three new "end-off" compartmental ligands, namely 2,6-bis(*N*-ethylmorpholine-iminomethyl)-4-R-phenol (R=-CH_3, Cl, ^{t}Bu) and of their correspondent zinc complexes in presence of thiocyanate as co-ligand. The complexes exhibit very

interesting photoluminescence properties, including room temperature phosphorescence, a very rare finding in Zn-SB complexes; moreover, the influence of the R substituent on these properties has been rationalized by DFT calculations. Structural analysis reveals the importance of $Zn(NCS)_4^{2-}$ anion for crystallization of the complexes and detailed DFT analysis justifies the role of R groups along with SCN to rationalize all the different non-covalent interactions which are very much significant for self-assembled dimerization in the solid state.

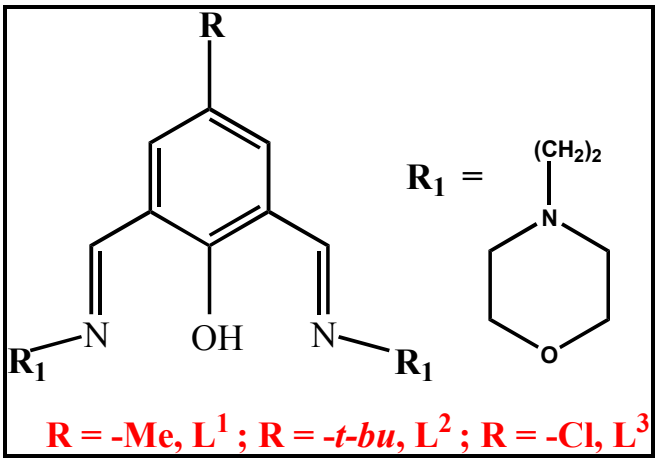

Scheme 1 Structure and labeling scheme for the three synthesized compartmental ligands.

Experimental section

Physical methods and materials

Elemental analyses (carbon, hydrogen and nitrogen) were performed using a Perkin–Elmer 240C elemental analyzer. Infrared spectra were recorded on KBr disks (400–4000 cm^{-1}) with a Perkin–Elmer RXI FTIR spectrophotometer. Electronic spectra were recorded on a Hitachi U-4010 spectrophotometer at 298 K. The steady state emission measurements were carried out using a Hitachi Model F-7000 spectrofluorimeter equipped with a 150 W xenon lamp, at 298 K using a stoppered cell of 1 cm path length. Emission studies at 77 K were made using a Dewar system having a 5 mm OD quartz tube and the freezing to 77 K of all the samples was achieved at the same rate. Phosphorescence spectra were recorded in a Hitachi Model F-7000 spectrofluorimeter equipped with phosphorescence accessories at 77 K.

Fluorescence quantum yield (Φ) was determined in each case by comparing the corrected emission spectrum of the samples with that of anthracene in MeOH (Φ 0.20)[23] using equation (1)[24] taking into account the total area under the emission curve.

$$Q = Q_R \frac{F}{F_R} \frac{OD_R}{OD} \frac{n^2}{n^2_R} \qquad (1)$$

where Q is the quantum yield of the compounds, F is the integrated fluorescence intensity (area under the emission curve), OD is the optical density, and n is the refractive index of the medium. It is assumed that the reference and the unknown samples are excited at the same wavelength (360 nm). The subscript R refers to the reference fluorophore (anthracene in this case) of known quantum yield. The standard quantum yield value was then used for the calculation of radiative and non-radiative rate constants of the systems.

Singlet state lifetimes were measured by a Time Master Fluorimeter from Photon Technology International (PTI, USA). The system consists of a pulsed laser driver PDL-800-B (from Pico-Quant, Germany) with interchangeable sub-nanosecond pulsed LEDs and pico-diode lasers (PicoQuant, Germany) with a TCSPC set-up (PTI, USA). The lifetimes of the free ligands and complexes were measured by using a diode laser LDH-405 (pulse width 200 ps) and PLS-370 (pulse width 600 ps) from PicoQuant, Germany, at a repetition frequency of 10 MHz. Instrument response functions (IRF) were measured at the respective excitation wavelengths of 370 nm (in the case of a LED) and 405 nm (in the case of a diode laser) using slits with a band pass of ~1-3 nm using Ludox silica as scatterer. Intensity decay curves were fitted as summation of exponential terms:

$$F(t) = \Sigma \alpha_i exp(-t/\tau_i)$$

The decay parameters were recovered using a non-linear iterative fitting procedure based on the Marquardt algorithm.[25] A deconvolution technique was used to determine the lifetime up to 150-200 ps with LED while the time resolution was 100 ps with diode laser. The quality of fit has been assessed over the entire decay, including the rising edge, and tested with a plot of weighted residuals and other

statistical parameters e.g., the reduced $\chi 2$ ratio and the Durbin– Watson (DW) parameters.[26]

The decay times of the three complexes in the milliseconds or longer range were also acquired by phosphorescence time-based acquisition mode in which emission intensity was measured as a function of time in the QM-30 fluorimeter (PTI, USA) using a gated detection system with start and end window time of 200 μs and 2000 μs, respectively. The decay parameters were recovered using a non-linear iterative fitting procedure based on the Marquardt algorithm.[26]

Anisotropy decay measurements were also carried out in Time Master Fluorimeter (PTI), USA using motorized Glen Thompson polarizer. The anisotropy, r(t) is defined as

$$r(t)=[\ Ivv\ (t)-G^{*}\ I_{VH}(t)]/[\ Ivv\ (t)+2^{*}\ G^{*}\ I_{VH}(t)]$$

where I(t) terms are defined as intensity decay of ESIPT emission of 3HNA with excitation polarizer orientated vertically and the emission polarizer oriented vertically and horizontally, respectively:

$$G = I_{HV}(t)/I_{HH}(t)$$

where G is the correction term for the relative throughput of each polarization through the emission optics. The entire data analysis was done with the software Felix 32 which analyses the raw data I_{VV} and I_{VH} simultaneously by global multi-exponential program and then the deconvolved curves (ID_{VV} and ID_{VH}) are used to construct r(t) [25] and from the fitted curve the correlation time (θ) can be recovered.

High purity *N*-(2-aminoethyl)morpholine was purchased from Sigma Aldrich chemical company and used as received. 2,6-diformyl-4-R-phenol (R= methyl, *tert*-butyl, chloro) were prepared according to the literature method.[27] Solvents were dried according to standard procedures and distilled prior to use. All other chemicals used were of AR grade.

Synthesis of the complexes

The following general template synthetic route was adopted for preparing all the complexes. The complexes **1**-**3** were prepared by treating a methanolic solution of zinc acetate with the Schiff-base formed *in situ* via condensation of 2, 6-diformyl-4-

R-phenol (where R= methyl, *tert*-butyl and chloro) with *N*-(2-aminoethyl)morpholine. The preparation, composition and physicochemical characteristics of all the complexes obtained using the template technique are given below.

$[Zn_2L^1(CH_3COO)_2][Zn(NCS)_4]$ (1). To a methanolic solution (5 mL) of *N*-(2-aminoethyl)morpholine (0.130 g, 1 mmol) a methanolic solution (10 mL) of 4-methyl-2,6-diformylphenol (0.184 g, 1mmol) was added in a dropwise manner and the mixture was refluxed for 1 hr. Then a methanolic solution (15 mL) of zinc acetate dihydrate (0.5475 g, 2.5 mmol) was added to it and reflux was continued for an additional 2 hrs. After cooling the mixture to ambient temperature a water-methanolic solution (5 mL) of sodium thiocyanate (0.246 g, 3 mmol) was added to it with stirring that was continued for further 2 h. The yellow solution thus obtained was kept in a $CaCl_2$ desiccator. Single crystals suitable for X-ray diffraction were separated out from the solution after two days. (Yield 85%). Anal. Calcd for $C_{54}H_{80}N_{12}O_{14}S_4Zn_5$: C(39.89%); H(4.96%); N(10.34%); Found C,(38.68%); H, (4.6%); N, (10.09%).

$[Zn_2L^2(CH_3COO)_2][Zn(NCS)_4]$(2). It was prepared by adopting the same procedure used for compound **1** using 4-*tert*-butyl-2,6-diformylphenol (0.206 g, 1 mmol) instead of 4-methyl-2,6-diformylphenol. Light yellow colored single crystals suitable for X-ray data collection were obtained from the filtrate after a week. (Yield 80%). Anal. Calcd for $C_{60}H_{86}N_{12}O_{14}S_4Zn_5$: C(43.51%); H(5.24%); N(10.15%); Found C,(43.35%); H, (4.98%); N, (10.12%).

$[Zn_2L^3(CH_3COO)_2][Zn(NCS)_4]$(3). It was prepared following the same procedure used for compound **1** replacing 4-methyl-2,6-diformylphenol with 4-chloro-2,6-diformylphenol(0.180 g, 1 mmol). Yellow colored single crystals suitable for diffraction were obtained from the filtrate after two days. (Yield 75%). Anal. Calcd for $C_{52}H_{68}Cl_2N_{12}O_{14}S_4Zn_5$: C(38.72%); H(4.25%); N(10.43%); Found C,(38.30%); H, (4.03%); N, (10.38%).

X-ray data collection and crystal structure determinations

The crystal structures of compounds **1**, **2** and **3** were determined by X-ray diffraction methods. Intensity data and cell parameters were recorded at 293(2) K on a Bruker APEX II equipped with a CCD area detector and a graphite monochromator (MoKα radiation λ = 0.71073 Å) The raw frame data were processed using SAINT and SADABS to yield the reflection data file.[28] The structures were solved by Direct Methods using the SIR97 program [29] and refined on F_o^2 by full-matrix least-squares

procedures, using the SHELXL-97 program [30] in the WinGX suite v.1.80.05.[31a] For compound **1**, the PLATON SQUEEZE procedure [31b] was used to treat regions of diffuse solvent which could not be sensibly modeled in terms of atomic sites. Their contribution to the diffraction pattern was removed and modified Fo^2 written to a new HKL file. The 47 electrons calculated by the program (void volume of 284.8 $Å^3$) correspond to six water molecules per cell, and were included in the formula, formula weight, calculated density, μ and F(000). All non-hydrogen atoms were refined with anisotropic atomic displacements except in the case of: i) two carbon atoms belonging to the ligand in **1** and ii) the disordered carbon atoms of the *tert*-butyl group in compound **2**. The hydrogen atoms were included in the refinement at idealized geometry (C-H 0.95 Å) and refined "riding" on the corresponding parent atoms. When possible, the solvent H-atoms were found in the difference Fourier map. The weighting schemes used in the last cycle of refinement were $w = 1/ [\sigma^2 F_o^2 + (0.1653P)^2 + 38.4826P]$, $w = 1/ [\sigma^2 F_o^2 + (0.1014P)^2 + 30.3288P]$, and $w = 1/ [\sigma^2 F_o^2 + (0.0822\ P)^2]$, where $P = (F_o^2 + 2F_c^2)/3$, for **1**, **2** and **3** respectively. Geometric calculations were performed with the PARST97 program.[32] Crystal data and experimental details for data collection and structure refinement are reported in Table 1.

Table 1 Crystal data and structure refinement information for compounds 1-3[c]

Compound	**1**	**2**	**3**
empirical formula	$C_{54}H_{80}N_{12}O_{14}S_4Zn_5$	$C_{60}H_{86}N_{12}O_{14}S_4Zn_5$	$C_{52}H_{68}Cl_2N_{12}O_{14}S_4Zn_5$
M	1624.39	1654.50	1611.17
crys syst	Monoclinic	Monoclinic	Triclinic
space group	*P2/n*	*C2/c*	*P-1*
a/Å	18.862(5)	37.918(4)	12.770(1)
b/Å	8.859(3)	13.384(1)	17.504(2)
c/Å)	22.798(6)	30.092(3)	17.798(2)

α/deg	-	-	64.249(5)
β /deg	111.291(3)	95.882(2)	72.721(1)
γ /deg	-	-	78.743(2)
V/Å^3	3549(2)	15191(2)	3411.4(6)
Z	2	8	2
T/K	293(2)	293(2)	293(2)
ρ /g cm^{-3}	1.520	1.447	1.569
μ /mm^{-1}	1.853	1.731	2.000
F(000)	1676	6848	1648
total reflections	22390	48859	11672
unique reflections (R_{int})	5880 (0.0590)	12102 (0.0721)	11672 (0)
observed reflections $[F_o>4\sigma(F_o)]$	3995	7372	6781
GOF on F^{2a}	1.005	1.037	1.047
R indices $[F_o>4\sigma(F_o)]^b R_1$, wR_2	0.0932, 0.3006	0.0654,0.1709	0.0581, 0.1431
largest diff. peak and hole (eÅ^{-3})	1.106, -0.579	1.009, -0.674	1.011, -0.425

[a]Goodness-of-fit S = [$\Sigma w(F_o^2-F_c^2)^2/(n-p)$]1/2, where n is the number of reflections and p the number of parameters. [b]$R_1 = \Sigma \| F_o | - | F_c \| / \Sigma | F_o |$, $wR_2 = [\Sigma[w(F_o^2-F_c^2)^2]/\Sigma[w(F_o^2)^2]]^{1/2}$.

[c] CCDC-1407549 -1407551 contain the supplementary crystallographic data for this paper.

Theoretical methods

The energies of the complexes studied in the non-covalent interactions study were computed at the BP86-D3/def2-TZVP level of theory. The geometries have been fully optimized unless otherwise noted. For instance to evaluate the non-covalent interactions observed in the solid state, we have used the crystallographic coordinates. The calculations have been performed by using the program TURBOMOLE version 6.5.[33] For the calculations we have used the BP86 functional with the latest available correction for dispersion (D3). [34]The basis set superposition error for the calculation of interaction energies has been corrected using the counterpoise method. For the spectroscopic studies, the geometries of the singlet ground state (S_0) and the lowest triplet excited state (T_1) for complexes **1**, **2** and **3** were optimized using the hybrid functional B3LYP in combination with the 6-31G* basis set for all atoms. Relativistic effects were included for the Zn atom by using the ECP-10-mdf Stuttgart/Dresden pseudopotential. The nature of the stationary points was confirmed by computing the Hessian at the same level of theory. All the geometry optimizations were carried out with the Gaussian09 program package. [35] The UV-Vis spectra were computed using TD-B3LYP using the same basis set as in the geometry optimizations. The phosphorescence emission spectra were simulated on the basis of ΔSCF-DFT calculations, which yield the energy difference between the triplet excited states at their optimized geometry and the closed-shell ground state at the same geometry in the gas phase. This latter approach is a simple but reliable way to determine emission energies. These calculations were performed in gas phase employing the same functional and basis set as in the optimizations. The phosphorescence radiative decay rates have been computed using QR TD-B3LYP calculations, as implemented in the Dalton program, [36] at the optimized geometries of the T_1 geometries of complexes **1** and **2**. The phosphorescence radiative decay rates constants (k_r) from one of the three spin sublevels (indexed by i) of the involved emissive states (T_m) can be expressed as

$$k_r^i = k_r(S_0, T_{em}^i) = \frac{4\alpha_0^3}{3t_0}\Delta E_{S-T}{}^3 \sum_{j\in\{x,y,z\}} \left|M_j^i\right|^2 \qquad (1)$$

Where $\Delta E_{S\text{-}T}$ is the transition energy, $t_0 = (4\pi\varepsilon_0)^2/m_e e^4$, α_0 is the fine-structure constant and M_j^i is the j axis projection of the electric dipole transition moment between the ground state and the i^{th} sublevel of the triplet state T_{em}. The M_j^i transition moment can be expressed as

$$M_j^i = \sum_{n=0}^{\infty} \frac{\langle S_0 | \hat{u}_j | S_n \rangle \langle S_n | \hat{H}_{SO} | T_{em}^i \rangle}{E(S_n) - E(T_{em})} + \sum_{n=0}^{\infty} \frac{\langle S_0 | \hat{H}_{SO} | T_n \rangle \langle T_n | \hat{u}_j | T_{em}^i \rangle}{E(T_n) - E(S_0)}, j \in \{x, y, z\} \quad (2)$$

Which is calculated by the QR TD-B3LYP calculation. The nonzero contribution to the $T_{em} \rightarrow S_0$ transition moment originates from the matrix elements of the electronic spin-orbit coupling operator ($\hat{H}_{SO}$) including summation over intermediate triplet states. Hence, the $T_{em} \rightarrow S_0$ transition borrows intensity from the spin-allowed $S_n \rightarrow S_0$ and $T_{em} \rightarrow T_n$ transitions. Note that individual phosphorescence rates for the three spin sublevels can be only experimentally in the limit of large fine-structure splittings and at low temperatures. At the high temperature limit, spin relaxation is usually fast and the triplet levels are almost equally populated. As a consequence, only weighted phosphorescence rates can be measured. Hence, phosphorescence rates are calculated according to (3).

$$k_r = \frac{1}{3} \sum_{i=1}^{3} k_r^i \quad (3)$$

From equations (1) and (3) we see that the phosphorescence rate is proportional to the cube of the emission energy and the square of the transition dipole moment. These calculations were done at the optimized T_1 geometries using the same basis sets as in the optimizations. The SOC operator used herein in all calculations makes use of a semi-empirical effective single-electron approximation, as suggested by Koseki et al.[37]

Results and discussion

Description of crystal structures

Complexes **1-3** were prepared reacting the ligand **HL-R** (with R equal to Me, ^{t}Bu and Cl, respectively) with zinc(II) acetate in methanol, in the presence of sodium thiocyanate. All complexes have general formula {2[Zn_2(**L-R**)$(CH_3COO)_2$][$Zn(NCS)_4$]}, comprising two cationic units [Zn_2(**L-R**)$(CH_3COO)_2]^+$ and the negative counterion $[Zn(NCS)_4]^{2-}$. The presence of a different substituent on the ligand does not affect the type of compound obtained from the structural point of view, as can be seen by the solid state analysis carried out through X-ray diffraction from single crystals.

The molecular structure of {2[$Zn_2(L^1)(CH_3COO)_2$][$Zn(NCS)_4$]·$3H_2O$} (**1**) is shown in Fig. 1. Crystallographic and refinement parameters are summarized in Table 1, and selected coordination bond lengths and angles are listed in Table 2. This structure is very similar to that of a previously reported complex [38] containing piperidine in the ligand instead of morpholine.

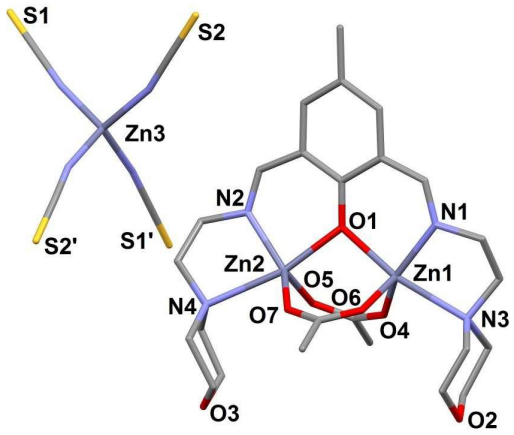

Fig. 1 Molecular structure of **1** with partial atom numbering scheme. Only one [$Zn_2(L^1)(CH_3COO)_2$] moiety is shown. Atoms S1' and S2' have been generated by symmetry. Hydrogen atoms have been omitted for clarity.

In the cationic unit, L acts as a dinucleating ligand through its four chelating nitrogen atoms and the bridging oxygen atom belonging to the phenoxide unit. The Zn(II) ions are also bridged by two acetate groups. The Zn−O and Zn−N bond distances are in normal ranges for these types of complexes. Zn1 and Zn2 are penta-coordinated, showing a geometry in between square-pyramidal and trigonal bipyramidal as evidenced by their tau-factors of 0.40 and 0.56, respectively (τ = 1 for a perfectly trigonal bipyramidal geometry, τ = 0 for a perfectly tetragonal geometry).[39]

Table 2 Selected Geometric Parameters (Å, °) for 1

Zn1–N1	2.004(9)	Zn3–N5	1.932(9)
Zn1–N3	2.358(9)	Zn3–N6	1.945(9)
Zn1–O1	2.073(8)	N3–Zn1–O1	168.3(4)

Zn1–O4	1.962(9)	N1–Zn1–O4	144.2(4)
Zn1–O6	1.981(7)	N1–Zn1–O6	109.5(3)
Zn2–N2	1.987(9)	O4–Zn1–O6	105.2(3)
Zn2–N4	2.4278(9)	N4–Zn2–O1	166.2(3)
Zn2–O1	2.100(8)	N2–Zn2–O5	114.7(4)
Zn2–O5	1.9689(8)	N2–Zn2–O7	132.2(4)
Zn2–O7	1.962(8)	O5–Zn2–O7	112.0(3)
Zn1-Zn2	3.262(2)		
Zn1–N1	2.004(9)	Zn3–N5	1.932(9)
Zn1–N3	2.358(9)	Zn3–N6	1.945(9)
Zn1–O1	2.073(8)	N3–Zn1–O1	168.3(4)
Zn1–O4	1.962(9)	N1–Zn1–O4	144.2(4)
Zn1–O6	1.981(7)	N1–Zn1–O6	109.5(3)
Zn2–N2	1.987(9)	O4–Zn1–O6	105.2(3)
Zn2–N4	2.4278(9)	N4–Zn2–O1	166.2(3)
Zn2–O1	2.100(8)	N2–Zn2–O5	114.7(4)
Zn2–O5	1.9689(8)	N2–Zn2–O7	132.2(4)
Zn2–O7	1.962(8)	O5–Zn2–O7	112.0(3)
Zn1-Zn2	3.262(2)		

The molecular structure of {2[$Zn_2(L^2)(CH_3COO)_2$][$Zn(NCS)_4$]} (**2**) is shown in Fig. 2. Crystallographic and refinement parameters are summarized in Table 1, and selected coordination bond lengths and angles are listed in Table 3.

Compound **2** crystallizes in the space group *C2/c*, and its asymmetric unit comprises two independent cationic complexes $[Zn_2(L^2)(CH_3COO)_2]^+$ (tagged with the letters A and B respectively) and the $[Zn(NCS)_4]^{2-}$ anion. Also in this case the structure is very similar to that of a previously reported complex formed with a pyrrolidine-based ligand. [38]

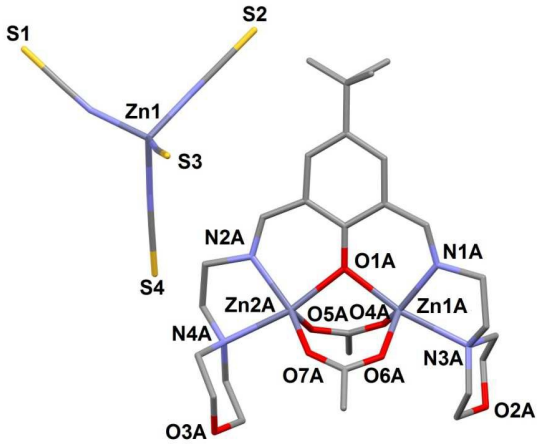

Fig. 2 Molecular structure of **2** with partial atom numbering scheme. Only one of the two independent $[Zn_2(L^2)(CH_3COO)_2]^+$ cations (tagged with the letter A) is shown. For the molecular structure of complex B, see ESI (Fig. S1). The labelling scheme for the two independent complexes is identical. Hydrogen atoms have been omitted for clarity.

Zn1A and Zn2A, are pentacoordinated, and also in this case their geometries lie in between a trigonal bipyramidal and square-pyramidal environment, as evidenced by the tau-factors of 0.59 that both ions display.

In the case of Zn1B and Zn2B, the geometry can be described as distorted trigonal bipyramidal (the tau-factors for the metal centres are 0.77 and 0.79) with axial angles of 169.5(2)° for both N3B-Zn1B-O1B and N4B-Zn2B-O1B. The axial positions of

the bipyramid are occupied by the phenoxide oxygen O1B and the morpholine nitrogens N3B and N4B (see Fig. S1),while the equatorial plane comprises one iminic nitrogen atom (N1B or N2B) and the oxygen atoms (O4B, O6B and O5B, O7B, respectively) of two distinct acetate ligands. The equatorial angles are very similar for the two ions, varying from roughly 117 to 123° (see Table 2).

Table 3 Selected geometric parameters (Å, °) for **2**

Zn1A–N1A	1.992(6)	Zn1B–N1B	1.980(7)
Zn1A–N3A	2.365(6)	Zn1B–N3B	2.306(8)
Zn1A–O1A	2.116(4)	Zn1B–O1B	2.100(5)
Zn1A–O4A	1.952(5)	Zn1B–O4B	1.951(6)
Zn1A–O6A	1.957(5)	Zn1B–O6B	1.939(5)
Zn2A–N2A	2.015(5)	Zn2B–N2B	1.983(8)
Zn2A–N4A	2.278(5)	Zn2B–N4B	2.301(8)
Zn2A–O1A	2.110(4)	Zn2B–O1B	2.109(5)
Zn2A–O5A	1.968(5)	Zn2B–O5B	1.945(6)
Zn2A–O7A	1.971(4)	Zn2B–O7B	1.951(5)
Zn1A-Zn2A	3.287(9)	Zn1B-Zn2B	3.236(1)
Zn1–N1	1.974(9)	Zn1–N3	1.965(9)
Zn1–N2	1.936(9)	Zn1–N4	1.952(9)
N3A–Zn1A–O1A	167.9(2)	N3B–Zn1B–O1B	169.5(2)
N1A–Zn1A–O4A	132.4(2)	N1B–Zn1B–O4B	117.1(3)
N1A–Zn1A–O6A	112.7(2)	N1B–Zn1B–O6B	119.3(3)

O4A–Zn1A–O6A	114.0(2)	O4B–Zn1B–O6B	123.4(3)
N4A–Zn2A–O1A	167.9(2)	N4B–Zn2B–O1B	169.5(2)
N2A–Zn2A–O5A	117.0(2)	N2B–Zn2B–O5B	118.3(3)
N2A–Zn2A–O7A	132.4(2)	N2B–Zn2B–O7B	122.3(3)
O5A–Zn2A–O7A	110.4(2)	O5B–Zn2B–O7B	119.3(3)

Reaction of the ligand L^3 with zinc(II) acetate in methanol, in the presence of sodium thiocyanate generates the complex $\{2[Zn_2(L^3)(CH_3COO)_2][Zn(NCS)_4]\}$ (**3**). The molecular structure of **3**, determined by single-crystal X-ray diffraction, is shown in Fig. 3. Crystallographic and refinement parameters are summarized in Table 1, and selected coordination bond lengths and angles are listed in Table 4.

Table 4 Selected geometric parameters (Å, °) for **3**

Zn1A–N1A	1.985(6)	Zn1B–N1B	1.991(6)
Zn1A–N3A	2.335(6)	Zn1B–N3B	2.391(6)
Zn1A–O1A	2.107(4)	Zn1B–O1B	2.116(4)
Zn1A–O4A	1.949(5)	Zn1B–O4B	1.982(5)
Zn1A–O6A	1.950(6)	Zn1B–O6B	1.941(6)
Zn2A–N2A	2.0034(5)	Zn2B–N2B	2.0226(5)
Zn2A–N4A	2.3064(7)	Zn2B–N4B	2.3403(5)
Zn2A–O1A	2.1014(4)	Zn2B–O1B	2.1045(4)
Zn2A–O5A	1.9591(6)	Zn2B–O5B	1.9776(5)
Zn2A–O7A	1.9464(4)	Zn2B–O7B	2.0039(6)
Zn1A-Zn2A	3.241(1)	Zn1B-Zn2B	3.2898(9)

Zn1–N1	1.950(7)	Zn1–N3	1.957(8)
Zn1–N2	1.956(8)	Zn1–N4	1.991(8)

N3A–Zn1A–O1A	169.0(2)	N3B–Zn1B–O1B	167.1(2)
N1A–Zn1A–O4A	116.9 (2)	N1B–Zn1B–O4B	105.6(2)
N1A–Zn1A–O6A	122.9 (2)	N1B–Zn1B–O6B	137.0(2)
O4A–Zn1A–O6A	119.6(2)	O4B–Zn1B–O6B	116.7(2)
N4A–Zn2A–O1A	167.6(2)	N4B–Zn2B–O1B	166.2(2)
N2A–Zn2A–O5A	125.0(2)	N2B–Zn2B–O5B	153.5(2)
N2A–Zn2A–O7A	120.8(2)	N2B–Zn2B–O7B	102.5(2)
O5A–Zn2A–O7A	113.9(2)	O5B–Zn2B–O7B	103.4(2)

As for **2**, the asymmetric unit comprises the two cationic complexes $[Zn_2(L^3)(CH_3COO)_2]^+$(tagged with the letters A and B) and the $[Zn(NCS)_4]^{2-}$ unit, which acts as negative counter ion and whose geometrical parameters are in the normal range for these type of systems.

As usual, Zn1A, Zn2A, Zn1B and Zn2B are penta-coordinated, but their geometries changed decidedly from distorted trigonal bipyramidal to distorted square-pyramidal, as evidenced by their tau-factors of 0.77, 0.71, 0.50 and 0.21, respectively. In the case of the bipyramidal Zn1A and Zn2A ions, the distorted geometry is revealed by the equatorial angles that vary from 116.9(2)° to 122.9(2)° (Zn1A) and from 113.9(2)° to 125.0(2)° (Zn2A). The tau value of 0.5 for Zn1B indicates a coordination environment that can either be described as tetragonal or trigonal bipyramidal. On the contrary, Zn2B is best described as square-pyramidal, with the acetate oxygen atom O7B in axial position and O1B-Zn2B-N4B (166.2(2)°) and N2B-Zn2B-O5B (153.5(2)°) forming the principal axis of the equatorial plane.

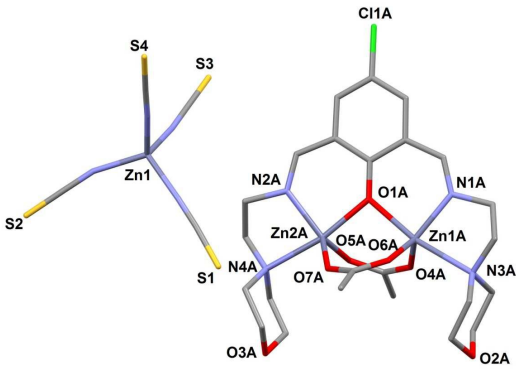

Fig. 3 Molecular structure of **3** with partial atom numbering scheme. Only one of the two independent $[Zn_2(L^3)(CH_3COO)_2]^+$ cations (tagged with the letter A) is shown. For the molecular structure of complex B, see ESI, Fig. S2. The labelling scheme for the two independent complexes is identical. Hydrogen atoms have been omitted for clarity.

In all three complexes the crystal structures are stabilized by i) weak CH···O hydrogen bonds mainly involving the oxygen atoms of the morpholine moieties and of the acetate groups; ii) stacking interactions between the phenoxide units of adjacent complexes; iii) CH···π interactions. The $[Zn(NCS)_4]^{2-}$complexes fill the remaining spaces in the lattice (see Supporting Information).

Absorption Spectra

The absorption spectra of the complexes **1**, **2** and **3** in methanol (MeOH) at room temperature are shown in Fig. 4. The maxima of different bands along with the ε values are provided in Table 5.

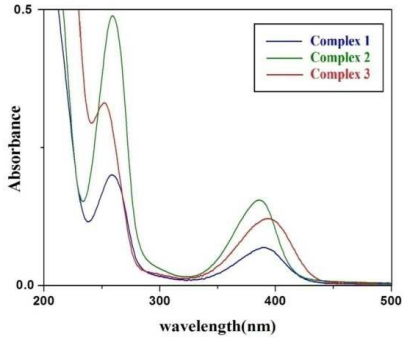

Fig. 4 Absorption spectra of three complexes (5×10^{-5} M) in methanol at 298K.

The lowest energy band of the complexes is observed around 390 nm. The bands are theoretically assigned as π-π^* excitations (see the TD-DFT UV-Vis spectra in Fig. S6-S7). It is also noted that maxima of the lowest energy bands remain almost same with change in solvent polarity (Table S1). The complex **2** and **3** exhibits higher absorbance compared to the complex **1**, indicating **2** and **3** exist as dimeric species in solution. (see later section)

Table 5 Absorption, steady state and time resolved fluorescence data at 298K and phosphorescence data at 298K and 77K of three complexes in methanol and in solid state.

Complex	$\lambda_{max}^{(A)}$ (nm) ε ($M^{-1}cm^{-1}$)		$\lambda_{max}^{(F)}$ (nm) [λ_{ex}=390nm] (relative fluorescence quantum yield,ϕ_F w.r.t. complex 3)	Singlet state lifetime monitoring the $\lambda_{max}^{(F)}$ [λ_{ex} =405 nm]				Rotational correlation time [θ_C (ns)] [λ_{ex}=370nm]	Phosphorescence spectra [λ_{ex}=390nm]			
				τ_1 (ns)	τ_2 (ns)	<τ> (ns)	χ^2		In methanol glass (77K)		In solid state (298K)	
									$\lambda_{max}^{(P)}$ (nm) (relative phosphorescence quantum yield,ϕ_P w.r.t. complex 2)	τ_p(s)	$\lambda_{max}^{(P)}$ (nm)	τ_p(ms)
1	259 (4200)	390 (1420)	446.0 (0.77)	0.77 (88.7%)	1.57 (11.3%)	0.87	1.0	2.69	497.0 (0.81)	0.47	512.0	0.53
2	259 (10270)	386 (3250)	441.0 (0.72)	0.54 (54.5%)	0.97 (45.5%)	0.73	1.0	4.16	490.0 (1.00)	0.54	505.0	0.60
3	252 (6940)	393 (2480)	455.0 (1.00)	1.20 (89.5%)	3.10 (10.5%)	1.39	1.0	4.85	506.0 (0.54)	0.22	510.0	0.47

Steady state and time resolved emission spectra

The fluorescence spectra of the three complexes in CH_3OH at room temperature are shown in Fig. 5 using λ_{exc}= 390 nm. The maxima of the emission bands and the relative quantum yield values of fluorescence of **1**, **2** and **3** are provided in Table S2. The complex **3** exhibits highest quantum yield. It is also noted that the chlorine analog shows a red shifted emission compared to methyl and tertiary butyl analog (Fig. 5,

Table 5). Excitation spectra of the complexes monitoring the corresponding $\lambda_{max}^{(F)}$ match well with their absorption spectra (Fig. 5).

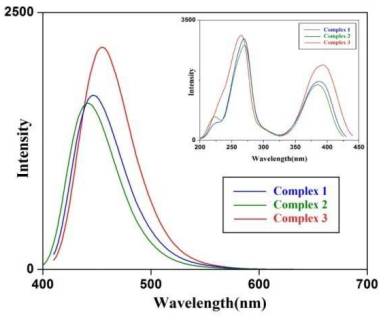

Fig. 5 Fluorescence spectra of three complexes in methanol at 298K; λ_{ex}=390nm; *Inset:* Excitation spectra of three complexes monitoring respective $\lambda_{max}^{(F)}$.

The fluorescence decay of the three complexes are shown in Fig. 6 with λ_{exc}= 405 nm. The decay in each case is found to fit with two exponentials (Table 5).

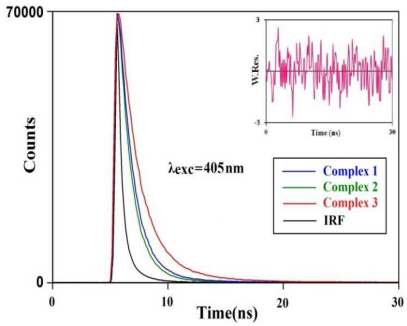

Fig. 6 Fluorescence decay of three complexes in methanol at 298K; λ_{exc} = 405 nm.

The average life times observed (Table 5) clearly corroborates the π-π* nature of the excited state. Complex **3** exhibits the longest average life time (1.39 ns) among the three complexes, in consistency with the observed highest quantum yield of **3**. The two components observed in the life time values could be due to the presence of two slightly different conformers of the complexes in the solution.

Anisotropy Study

Time resolved anisotropy decay monitoring the $\lambda_{max}^{(F)}$ of **1**, **2** and **3** were performed (Fig.7) in methanol solvent and the recovered rotational correlation time (θ_C) is provided in Table 4. The θ_C values for **2** and **3** are found to be almost double

compared to that observed in **1**. This is a clear indication that **2** and **3** exist in dimeric species in solution.

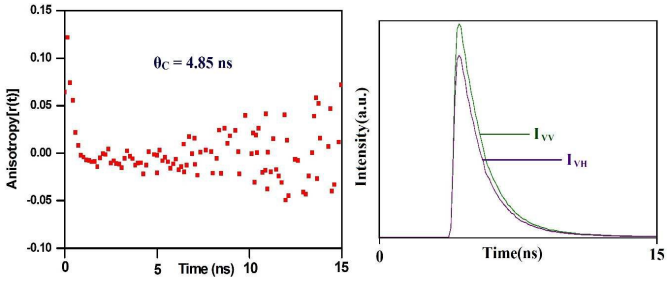

Fig. 7 Time resolved anisotropy decay of **Complex 3** (0.5 μM) at 298 K in methanol. I_{VV} and I_{VH} represent decays of emission of complex **3** with excitation polarizer at vertical position and emission polarizer at vertical and horizontal position respectively. **λ_{ex}=370nm**; excitation and emission band pass = 10 nm each.

Phosphorescence Spectra

The low temperature total emission spectra and low temperature phosphorescence spectra of the three complexes in methanol glass at 77K (λ_{ex}=390 nm) are shown in Fig. 8(A) and 8(B) respectively. The phosphorescence maxima and lifetimes of the three complexes are shown in Table 5.

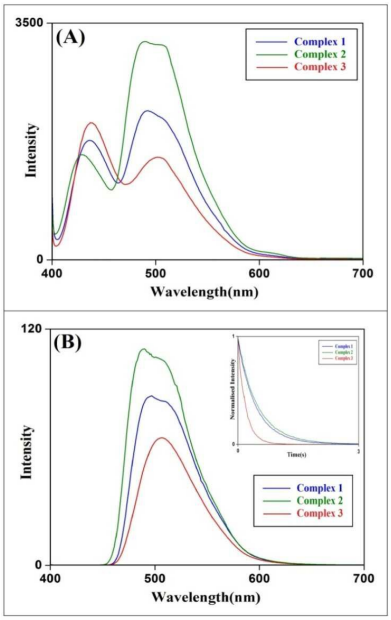

Fig. 8 (A) Low temperature total emission spectra of three complexes in methanol glass at 77K.λ_{ex}=390nm. (B)Low temperature phosphorescence spectra of three complexes in methanol glass at 77K, λ_{ex}=390 nm; Excitation and emission band-pass

= 10 nm and 2.5 nm, respectively. *Inset:*Phosphorescence decay of three complexes in methanol glass at 77K; λ_{ex}= 390 nm; all the solutions have optical density= 0.2.(please see)

The values of phosphorescence life time further demonstrate the π-π^* nature of the lowest triplet in each case. Indeed, an analysis of the UB3LYP spin density distributions (see exemplarily for complexes **2** and **3** in Fig. 9) reveals a lesser participation of the Zn atom in the emission process for all complexes. In Table 5 are reported the computed phosphorescence emission maxima for complexes **1-3** in base of ΔSCF-B3LYP calculations (see Computational methods). The agreement with the experiment is remarkable. It is noted that the phosphorescence quantum yield is in the order t-Bu>Me>Cl. Furthermore, the t-Bu and Me analogs exhibit vibronic structure in their spectra at 77K. The life time values of the triplet state are consistent with the intensity of the phosphorescence of the complexes. The phosphorescence quantum yield can be expressed as $\Phi_{phos}= \Phi_{ISC}k_r\tau_{phos}$ (4), where Φ_{ISC} is the intersystem crossing (ISC) efficiency, k_r is the radiative phosphorescence decay rate and τ_{phos} is the phosphorescence lifetimes. To gain insight into these processes we have computed the radiative rates for complexes **1-2** using QR TD-B3LYP calculations (see computational details). Both complexes possess very similar k_r values, being 1.11 the k_3 ($T_1 \rightarrow S_0$) /k_2 ($T_1 \rightarrow S_0$) ratio. Due to the similar i) values for the measured singlet-triplet gaps and the ii) expected SOCs for all the complexes, similar Φ_{ISC} values are also expected. [40a] Due to the similar ISC and radiative processes, the phosphorescence lifetime is the ultimate factor governing the phosphorescence quantum efficiency of complexes **1-3** (see Eq. 4). Indeed, as seen in Table 4, the lifetime values of the triplet state are consistent with the intensity of the phosphorescence of the complexes. The agreement with the experiment is remarkable.

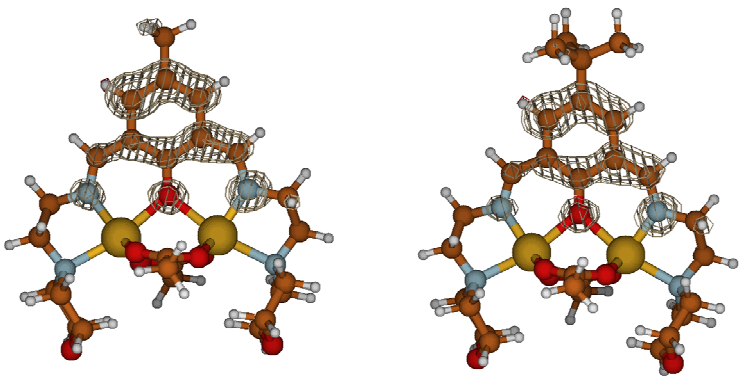

Fig. 9 Spin density distribution (B3LYP/6-31G*) plots at the lowest triplet (T_1) optimized minimum structures of complexes **2** and **3**.

Table 6 Computed phosphorescence emission maxima and k_r values.

	Complex **1**	Complex **2**	Complex **3**
ΔSCF-B3LYP/6-31G* [eV(nm)]	2.15 (577)	2.19 (566)	2.21 (562)

The room temperature total emission spectra along with the phosphorescence spectra of three complexes in transparent potassium bromide (KBr) medium (λ_{ex}=390nm) are shown in Fig. 10 (Table 6), where the intensity of phosphorescence of the complexes is in the same order as observed in the glassy matrix.

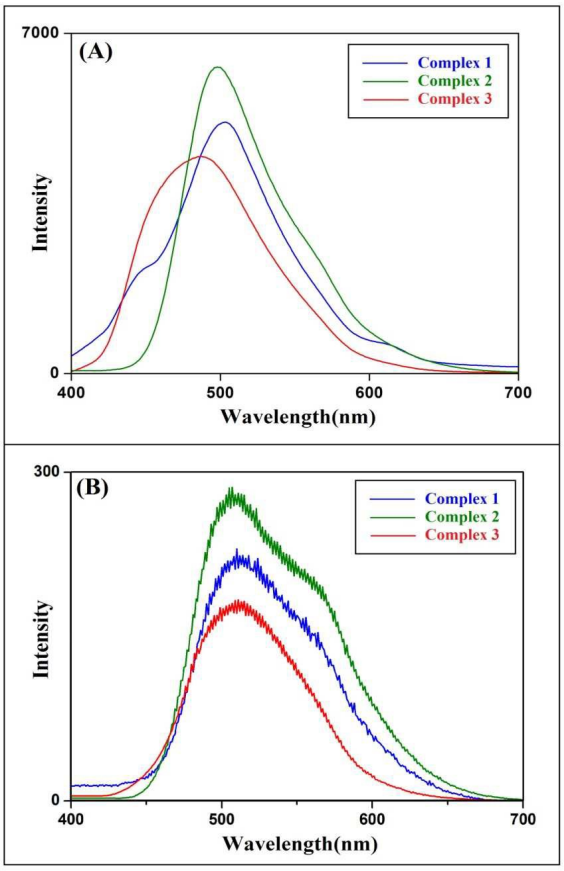

Fig. 10 (A) Room temperature total emission spectra of three complexes in transparent KBr medium at 298K; λ_{ex}=390nm; (B) Room temperature

phosphorescence spectra of three complexes in solid state at 298K, λ_{ex}=390 nm; Excitation and emission band-pass = 10 nm and 2.5 nm, respectively.

It is worth noticing that the complexes exhibit phosphorescence at room temperature in solid state. This observation implies that either the ligands are rigidly held by metal ions in all the complexes or there could be distortion in the geometry of the triplet state [40b] or both.

Theoretical study on weak interactions

We have analyzed the influence of the para substituent on the solid state architecture of complexes **1-3** (see Fig. 11). It should be mentioned that the dinuclear $Zn_2L(OAc)_2$ complex is cationic and two complexes are compensated by one dianionic $[Zn(NCS)_4]^{2-}$ moiety. Therefore the non-covalent interactions in the solid state are mainly governed by strong electrostatic between counter ions. We have intended to evaluate the contribution of other weak and more directional non-covalent interactions using theoretical models based on the X-ray structures. Experimentally, solid state structures are only formed if SCN^- is present in the reaction medium. Therefore the presence of the $[Zn(NCS)_4]^{2-}$ dianion is a requirement for crystallization. We have also analyzed theoretically the different interactions where the dianion participate in the three structures. The dual electron σ-donor/π-acceptor ability of the SCN ligands is crucial to understand the different complexes observed in the solid state.

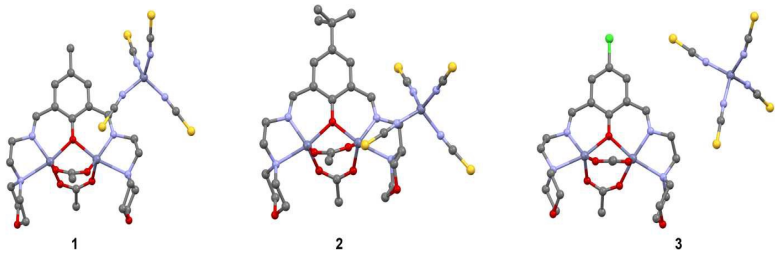

Fig. 11 Partial view of the X-ray structures **1**–**3**. Only one cationic unit is represented.

We have first computed the molecular electrostatic potential of $Ti(NCS)_4$ complex as a neutral model of the anionic part in order to analyze the electron donor/acceptor ability of the NCS ligand in the absence of strong electrostatic effects. The MEP surface is represented in Fig. 12 and it is worth mentioning some interesting aspects. There is a σ-hole at the sulfur atom (at extension of the C=S bond) and a negative belt around the sulfur atom, therefore it can participate in both hydrogen bonding and

chalcogen bonding interactions. In addition, the nitrogen atom can also participate in hydrogen bonding interactions as acceptor.

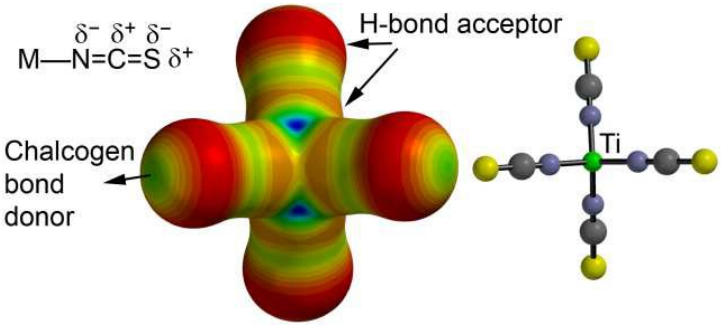

Fig. 12 Molecular electrostatic potential of the $Ti(NCS)_4$ complex.

We have examined the solid state structure of compounds **1**–**3** focusing the attention on the $[Zn(NCS)_4]^{2-}$ moiety and we have found some interesting complexes that give reliability to the above-mentioned MEP analysis and the ability of the NCS ligand to participate in different interactions. As representative example, we show in Fig. 13 two fragments of compound **1** (left) and **3** (right). In compound **1** the $[Zn(NCS)_4]^{2-}$ moiety bridges two cationic complexes by means of chalcogen S···O interactions. In compound **3** it bridges two complexes by means of a bifurcated C–H···N hydrogen bond and a lone pair(lp)–π interaction involving the negative belt of one sulphur atom. We have computed the interaction energies of both fragments and they are very large and negative due to the strong ion pair interactions (ΔE_1 = –143.4 and ΔE_2 = –179.1 kcal/mol for **1** and **3**, respectively). In an effort to compute the contribution of these interactions in the absence of these strong electrostatic effects, we have used neutral dimeric models. In the cationic complex we have changed one acetate ligand by a carbonate and the anionic complex $[Zn(NCS)_4]^{2-}$ has been replaced by $Ti(NCS)_4$. The models and energetic results are shown in Fig. 14. The interaction energies are considerably reduced to ΔE_3 = –15.7 kcal/mol for the chalcogen bonding and ΔE_4 = –20.4 kcal/mol and ΔE_5 = –17.8 kcal/mol for the hydrogen bonding and anion–π interactions, respectively.

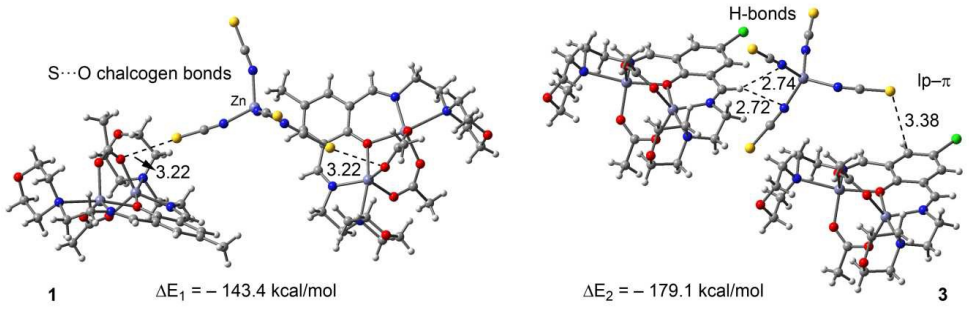

Fig. 13 Partial views of x-ray structures **1** and **3**. Distances in Å.

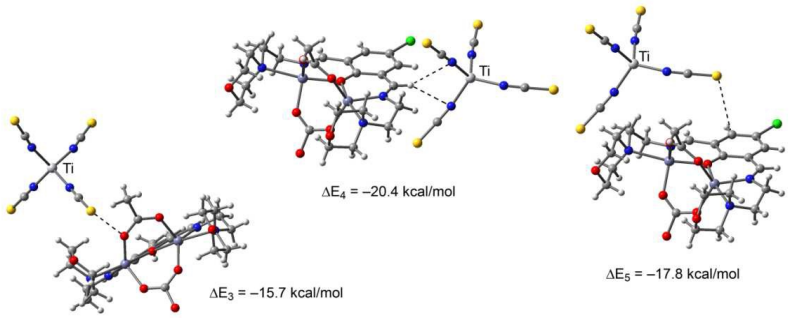

Fig. 14 Dimeric neutral models used to evaluate the non-covalent interactions involving the SCN ligand.

In addition to these theoretical considerations regarding the dual behavior of the coordinated NCS ligand, we have analyzed the influence of the *para* substituent of the aromatic ligand on the solid state structures. We have found that the three complexes form similar self-assembled dimers in the solid state with different participation of the para substituent (see Fig. 15). That is, the methyl group in compound **1** establishes weak C–H···O interactions, the *t*-butyl group in **2** participates in a great number of weak C–H/π interactions and the chlorine substituent in **3** establishes hydrogen and halogen bonding interactions. The main difference is that in compound **2**, π –π stacking interactions are not formed, influencing the final solid state architecture of the compound. We have analyzed the energetic features of these interactions using the models shown in Fig. 15. We have used neutral models where one acetate ligand has been replaced by carbonate. In addition, for each self-assembled dimer, we have computed the interaction energy of a theoretical model where the substituent has been replaced by a hydrogen atom. This procedure allows estimating the contribution of the substituent on the total interaction energy. The energetic results are also shown in Fig.

15 where the theoretical model (Me→H) for compound **1** as representative example is also represented (top-right). Interestingly the dimerization energies are similar for all compounds (≈ –13 kcal/mol), however the contribution of the substituent is different. In the dimers of compounds **1** and **3**, in addition to the interaction that involves the substituent, there is also a contribution of a π–π stacking interaction (π–π distances are 3.645 Å and 3.593 Å for **1** and **3** respectively, measured from the ring centroid of one ring to the mean plane of the other ring). A similar π–π stacking interaction is not possible in compound **2** due to the formation of multiple C–H/π interactions involving the ^{t}Bu substituent. The interaction energies computed for compounds **1** and **3** (ΔE_6 = –13.1 kcal/mol and ΔE_8 = –12.6 kcal/mol, respectively) are significantly reduced to $\Delta E_6'$ = –7.2 kcal/mol and $\Delta E_8'$ = –6.2 kcal/mol when the substituent in *para* is replaced by a hydrogen atom. Consequently, the contribution of the C–H···O interactions is $\Delta E_6 - \Delta E_6'$ = –5.9 kcal/mol in **1** and the contribution of the Cl···O and Cl···H interactions in **3** is $\Delta E_8 - \Delta E_8'$ –6.4 kcal/mol. In compound **2**, the dimerization energy is basically due to the multiple C–H/π interactions established by the *t*-butyl groups in *para* since the value of $\Delta E_7'$ is negligible. Keeping in mind that many other interactions are present in the solid state, this energetic analysis focused only on the interactions involving the *para* substituent is useful to understand the different architecture adopted by compound **2** (compared to **1** and **3**) since the dimer formation is governed only by C–H/π interactions .

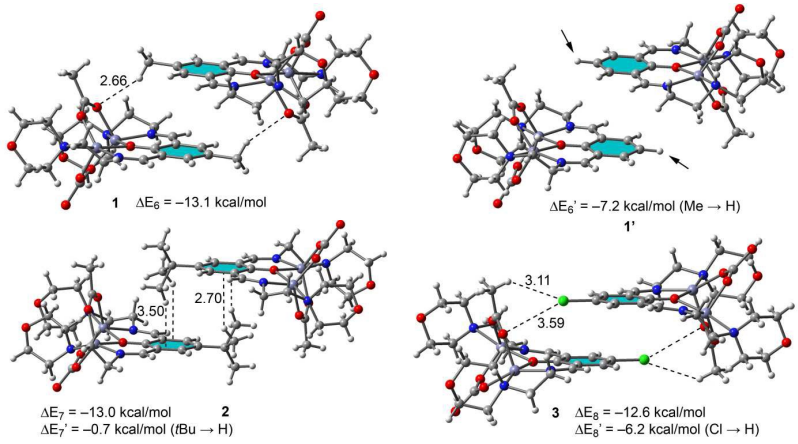

Fig. 15 Dimeric neutral models used to evaluate the noncovalent interactions involving the para substituent in compounds **1**–**3**. Distances in Å.

Conclusions

Three phenol based "end-off" compartmental ligands, namely 2,6-bis(*N*-ethylmorpholine-iminomethyl)-4-R-phenol (R=-CH_3, Cl, ^{t}Bu) have been designed and synthesized. Zn(II) complexes of those ligands have been prepared in presence of SCN as coligand and structurally characterized through single crystal X-ray diffraction analysis. All the complexes exhibit very similar structural features: a dinuclear cationic complex $[Zn_2L(CH_3COO)_2]^{2+}$ with $Zn(NCS)_4^{2-}$ as counter anion. Experimental evidences and DFT calculations suggest the presence several weak interactions in all three complexes. Theoretical analysis using neutral dimeric model unambiguously verify the importance of SCN group in stabilizing the complexes. DFT calculations also establish the influence of R group; i.e., para substituent in controlling the weak interaction and thereby making slightly different architecture in three cases. Photoluminescence property of the complexes has been explored by extensive experimental investigation followed by detailed DFT calculations and thereby the origin of the photoluminescence behavior of our designed Schiff-base complexes of Zn(II), one of the prime themes of this work, has been rationalized. All the three complexes show phosphorescence at room temperature, a rare finding in zinc Schiff-base photochemistry, and the role of para substituents on phosphorescence efficiency has been authenticated by DFT calculations.

Acknowledgement

The authors wish to thank CSIR, New Delhi [01(2464)/11/EMRII dt 16-05-11 to D.D.] for financial support and the University of Calcutta for providing the facility of a single crystal X-Ray diffractometer from the DST-FIST program. This work was supported by the DGICYT of Spain (project CONSOLIDER INGENIO 2010 CSD2010-00065, FEDER funds). S.G. gratefully acknowledges CSIR (no. 21(0871)/11/EMR-II), DST (no.SR/S1/PC-57/2008), and DST (no. SB/S1/PC-003/2013) for financially supporting this work. S.S. thanks CSIR for the SRF fellowship (no. 21(0871)/11/EMR-II).

References

1 H. Vahrenkamp, *Chem. Unserer Zeit.,* 1988, **22**, 73.

2 J. J. Frau´sto da Silva, R. J. P. Williams, *The Biological Chemistry of the Elements*; Clarendon Press: Oxford, 1991; p 302.

3 J. M. Berg, Yi. Shi, *Science*, 1996, **271**, 1081.

4 W. N. Lipscomb, N. Stra¨ter, *Chem. Rev*. ,1996**, 96**, 2375.

5 A. Takeda, *BioMetals*, 2001, **14**, 343.

6 T. Valente, C. Auladell, *Mol. Cell. Neurosci*., 2002, **21**, 189.

7 S . C. Burdette, S. J. Lippard, *Proc. Natl. Acad. Sci. USA.*2003, **100**, 3605.

8 G. Parkin, *Chem. Rev.,* 2004, **104***,* 699.

9 P. Jiang, Z. Guo, *Coord. Chem. Rev.,* 2004, **248,** 205.

10 M. Maiti, S. Thakurta, D. Sadhukhan, G. Pilet, G. M. Rosair , A. Nonat , L. J. Charbonnière , S. Mitra , *Polyhedron,* 2013, **65**, 6.

11 S. Mizukami, H. Houjou, Y. Nagawa, M. Kanesato, *Chem. Commun.,* 2003, 1148.

12 H. Kunkely, A. Vogler, *Inorg. Chim. Acta*., 2001**, 321**, 171.

13 K. H. Chang, C. C. Huang, Y. H. Liu, Y. H. Hu, P. T. Chou, Y. C. Lin, *Dalton Trans.,* 2004, 1731.

14 C. M. Che, S.C. Chan, H.F. Xiang, M.C.W. Chan, Y. Liu, Y. Wang, *Chem. Commun*., 2004, 1484.

15 P. Chakraborty, J. Adhikary, S. Samanta, D. Escudero, A.C. Castro, M. Swart, S. Ghosh, A. Bauza, A. Frontera, E. Zangrando, D. Das, *Cryst. Growth Des.,* 2014, **14**, 4111.

16 K. Ehama, Y. Ohmichi, S. Sakamoto, T. Fujinami, N. Matsumoto, N. Mochida, T. Ishida, Y. Sunatsuki, M.Tsuchimoto, N. Re, *Inorg. Chem*., 2013, **52**, 12828.

17 C. Maxim, F. Tuna, A.M. Madalan, N. Avarvari, M. Andruh, *Cryst. Growth Des*., 2012, **12**, 1654.

18 M. Yamamura, H. Miyazaki, M. Iida, S. Akine, T. Nabeshima, *Inorg. Chem*., 2011, **50**, 5315.

19 C.C. Roberts, B.R. Barnett, D.B. Green, J.M. Fritsch, *Organometallics*, 2012, **31,** 4133.

20 M. Prabhakar, P. S. Zacharias, S. K. Das, *Inorg. Chem.*, 2005, **44**, 2585.

21 K. Dhara, S. Karan, J. Ratha, P. Roy, G. Chandra, M. Manassero, B. Mallik, P. Banerjee, *Chem. Asian J*., 2007, **2**, 1091.

22 B. Dutta, P. Bag, U. Flo1rke, K. Nag, *Inorg. Chem*., 2005, **44**, 147.

23 P. Hrdlovic, J. Donovalova, H. Stankovicova, A. Gaplovsky, *Molecules*, 2010,**15**, 8915.

24 Lakowicz, J.R. (Eds.) "Principles of Fluorescence Spectroscopy", 3rd Edition, Kluwer Academic/ Plenum Publishers: New York, 2003.

25 P. R. Bevington, Data Reduction and Error Analysis for the Physical Sciences, McGraw Hill, New York, 1969, pp. 235.

26 (a) FELIX 32, Operation Manual, Version 1.1, Photon Technology International, Inc., NJ, 2003; (b) FELIX GX, Operation Manual, Version 2.0.1, Photon Technology International, Inc., NJ, 2003. 29. FELIX 32, Operation Manual, Version 1.1, Photon Technology International Inc, NJ, 2003.

27 R. R. Gagne, C.L. Spiro, T.J. Smith, C.A. Hamann, W.R. Thies, A.K. Shiemeke, *J.Am. Chem. Soc.,* 1981, **103**, 4073.

28 SADABS Bruker AXS; Madison, Wisconsin, USA, 2004; SAINT, *Software Users Guide*, *Version 6.0*; Bruker Analytical X-ray Systems, Madison, WI (1999). G. M. Sheldrick, SADABS v2.03: *Area-Detector Absorption Correction*. University of Göttingen, Germany (1999).

29 A. Altomare, *J. Appl. Cryst*. 1999, **32**,115.

30 Sheldrick, G. M. *SHELXL-97.Program for Crystal Structure Refinement*. University of Göttingen, Germany, 1997 and *Acta Crystallogr*. 2008, **A64**,112.

31 (a) L. J. Farrugia, *J.Appl. Crystallogr*. 1999, **32**, 837; (b) P. v.d. Sluis, A. L. Spek, *Acta Cryst., Sect A*. 1990, **46,** 194.

32 M. Nardelli, *J. Appl. Crystallogr.* 1996, **29**, 296.

33 R. Ahlrichs, M. Bär, M. Hacer, H. Horn, C. Kömel, *Chem. Phys. Lett.,* 1989, **162,** 165.

34 S. Grimme, J. Antony, S. Ehrlich, H. Krieg, *J. Chem. Phys*., 2010, **132**,154104.

35 Gaussian 09, Revision A.1, M. J. Frisch, G. W. Trucks, H. B. Schlegel, G. E. Scuseria, M. A. Robb, J. R. Cheeseman, G. Scalmani, V. Barone, B. Mennucci, G. A. Petersson, H. Nakatsuji, M. Caricato, X. Li, H. P. Hratchian,

A. F. Izmaylov, J. Bloino, G. Zheng, J. L. Sonnenberg, M. Hada, M. Ehara, K. Toyota, R. Fukuda, J. Hasegawa, M. Ishida, T. Nakajima, Y. Honda, O. Kitao, H. Nakai, T. Vreven, J. A. Montgomery, Jr., J. E. Peralta, F. Ogliaro, M. Bearpark, J. J. Heyd, E. Brothers, K. N. Kudin, V. N. Staroverov, R. Kobayashi, J. Normand, K. Raghavachari, A. Rendell, J. C. Burant, S. S. Iyengar, J. Tomasi, M. Cossi, N. Rega, J. M. Millam, M. Klene, J. E. Knox, J. B. Cross, V. Bakken, C. Adamo, J. Jaramillo, R. Gomperts, R. E. Stratmann, O. Yazyev, A. J. Austin, R. Cammi, C. Pomelli, J. W. Ochterski, R. L. Martin, K. Morokuma, V. G. Zakrzewski, G. A. Voth, P. Salvador, J. J. Dannenberg, S. Dapprich, A. D. Daniels, Ö. Farkas, J. B. Foresman, J. V. Ortiz, J. Cioslowski, and D. J. Fox, Gaussian, Inc., Wallingford CT, **2009**.

36 T. Helgaker, H. J. Aa. Jensen, P. Jørgensen, J. Olsen, K. Ruud, H. Ågren, A. A. Auer, K. L. Bak, V. Bakken, O. Christiansen, S. Coriani, P. Dahle, E. K. Dalskov, T. Enevoldsen, B. Fernandez, C. Hättig, K. Hald, A. Halkier, H. Heiberg, H. Hettema, D. Jonsson, S. Kirpekar, R. Kobayashi, H. Koch, K. V. Mikkelsen, P. Norman, M. J. Packer, T. B. Pedersen, T. A. Ruden, A. Sanchez, T. Saue, S. P. A. Sauer, B. Schimmelpfennig, K. O. Sylvester-Hvid, P. R.Taylor, O. Vahtras, *Dalton, a Molecular Electronic Structure Program, Release 1.2*. 2001.

37 S. Koseki, M. Schmidt, M. Gordon, *J. Phys. Chem.,* 1990, **96**, 10678.

38 P. Maiti, A. Khan, T. Chattopadhyay, S. Das, K. Manna, D. Bose, S. Dey, E. Zangrando, D. Das, *J. Coord. Chem*., 2011, **64**, 3817.

39 A. W. Addison, T. N. Rao, J. Reedijk, J. Vanrijn, G. C. Verschoor, *J. Chem. Soc. Dalton Trans.,* 1984, 1349.

40 (a) D. Escudero, D. Jacquemin, *Dalton Trans.,* 2015, **44,** 8346; (b) A.J. Howarth, R. Patia, D.L. Davies, F. Leji, M.O. Wolf, K. Singh, *Eur. J. Inorg. Chem.,* 2014*,* 3657.

Graphical Abstract

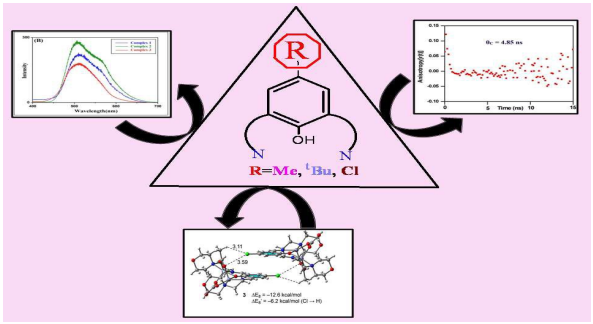

How the para substituents (R) of phenol based "end-off" compartmental ligands may be instrumental in controlling the energetic features of different non-covalent interactions present in crystal structure and photoluminescence behavior of dinuclear zinc complexes have been investigated experimentally and theoretically.